ACS APPLIED MATERIALS & INTERFACES

Research Article

www.acsami.org

Hyper-Branched Cu@Cu_2O Coaxial Nanowires Mesh Electrode for Ultra-Sensitive Glucose Detection.

Yuxin Zhao,[†] LiLi Fan,[§] Ying Zhang,[‡] Hu Zhao,[∥] Xuejin Li,[‡] Yanpeng Li,[‡] Ling Wen,[‡] Zifeng Yan,*[,‡] and Ziyang Huo*[,⊥]

[†]State Key Laboratory of Safety and Control for Chemicals, SINOPEC Safety Engineering Institute, No 218, Yan'an 3 road, Shinan District, Shandong, Qingdao 266071, China

[‡]State Key Laboratory for Heavy Oil Processing, PetroChina Key Laboratory of Catalysis, and [§]Department of Chemistry, College of Science, China University of Petroleum (East), Qingdao 266580, China

[∥]Domestic Division, China Petroleum Pipeline Bureau, 87 Guangyang Road, Hebei, Langfang 065000, China

[⊥]Queensland Micro- and Nanotechnology Centre Nathan Campus, Griffith University, 170 Kessels Road, Nathan Queensland 4111, Australia

Supporting Information

ABSTRACT: Electrode design in nanoscale is expected to contribute significantly in constructing an enhanced electrochemical platform for a superb sensor. In this work, we present a facile synthesis of new fashioned heteronanostructure that is composed of one-dimensional Cu nanowires (NWs) and epitaxially grown two-dimensional Cu_2O nanosheets (NSs). This hierarchical architecture is quite attractive in molecules detection for three unique characteristics: (1) the three-dimensional hierarchical architecture provides large specific surface areas for more active catalytic sites and easy accessibility for the target molecules; (2) the high-quality heterojunction with minimal lattice mismatch between the built-in current collector (Cu core) and active medium (Cu_2O shell) considerably promotes the electron transport; (3) the adequate free space between branches and anisotropic NWs can accommodate a large volume change to avoid collapse or distortion during the reduplicative operation processes under applied potentials. The above three proposed advantages have been addressed in the fabricated Cu@Cu_2O NS-NW-based superb glucose sensors, where a successful integration of ultrahigh sensitivity (1420 μA mM^{-1} cm^{-2}), low limit of detection (40 nM), and fast response (within 0.1 s) has been realized. Furthermore, the durability and reproducibility of such devices made by branched core−shell nanowires were investigated to prove viability of the proposed structures. This achievement in current work demonstrates an innovative strategy for nanoscale electrode design and application in molecular detection.

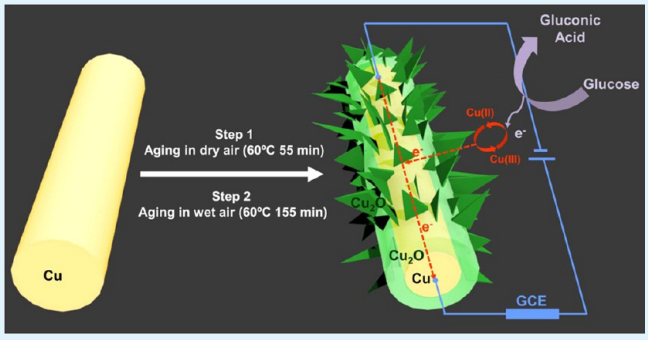

KEYWORDS: *nanowires, glucose sensor, hierarchical structures, core−shell, epitaxial growth*

1. INTRODUCTION

Since the pioneering work on glucose enzyme electrodes in 1962, tremendous academic and commercial efforts has been directed toward developing electrochemical glucose sensors not only because of their great promise in medical diagnosis and diabetes management but also the increasing demands for bioprocess/environmental monitoring, beverage industry, and pharmaceutical analysis.[1−3] To date, there are essentially two categories of electrochemical glucose sensors: enzymatic and nonenzymatic noble metal-modified sensors. However, these sensors usually suffer from poor stability caused by the intrinsic nature of enzymes and intermediates/pollutants poisoning.[4−8] Many efforts have been made to overcome these problems and the recent research of hotspots is focus on exploration of enzyme-free glucose sensors though utilizing inexpensive and resourceful transition-metal catalysts. Thereby a fair amount of nanostructured electrodes have been extensively used to form innovative nonenzymatic sensors.[9−14]

Branched nanowires (NWs), one of the most promising three-dimensional (3D) hierarchically structured nanomaterials, has recently been drawn considerable attention in chemical and biological electroanalysis due to their unique properties from the interesting combination of the primary one-dimensional (1D) structure and secondary attaching structures.[15] Moreover, the smart integration of different materials in nanoscale can create more homogeneous/heterogeneous junctions and large surface area to gain the novel functions and improve performance which cannot be realized from each of the

Received: May 27, 2015
Accepted: July 17, 2015
Published: July 17, 2015

DOI: 10.1021/acsami.5b04614
ACS Appl. Mater. Interfaces 2015, 7, 16802−16812

Scheme 1. Two-Step Synthesis Process for Hierarchical Cu@Cu_2O NS-NW Nanostructures and Its Application in Glucose Monitoring

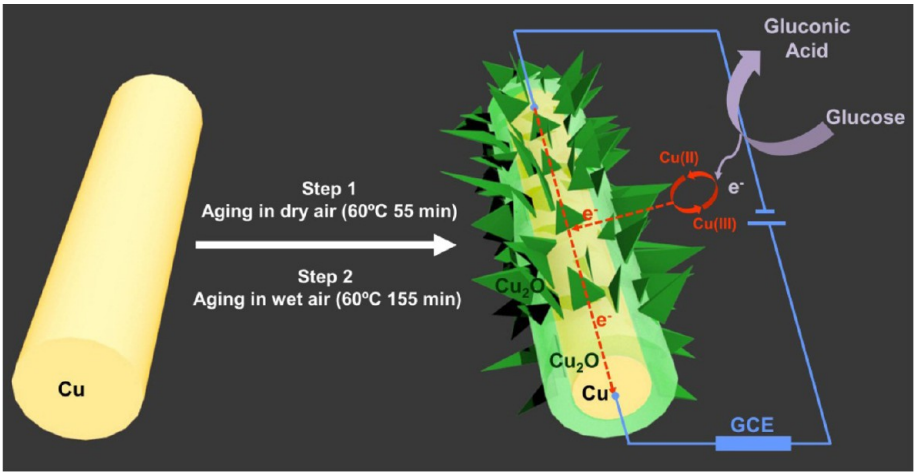

components separately.[16−19] For superb performance enzymeless glucose sensors, such 3D material offers several potential advantages as the following: (i) 1D NW backbone effectively shortens the electron-tunneling distance to promote direct electron transfer between the electrode and immobilized analytes, facilitating rapid response and superior sensitivity.[20−23] (ii) The large superficial area of 3D branched NW structures ensures adequate active sites and allows easy access of detected species to accelerate the kinetics of electro-oxidation of glucose for enhanced electroactivity.[24,25] (iii) The space between neighboring branches plays as an elastic buffer for the aggregation and collapse after numerous reduplicative measurements under applied potential, effectively ensuring the desirable reproducibility and stability of performance.[26,27] Up to now, enormous efforts have first focused on the rational synthesis of branched heterostructure NWs from postgrowth strategy involving gas-phase chemical vapor deposition (CVD),[28−30] sol−flame techniques,[31] electrodeposition,[32] etc. However, these approaches usually include expensive apparatus and multiple steps, which evidently increase complexity in synthetic procedures and limit large-scale production. Therefore, the effective and durable fabrication of an integrated smart architecture with less interface defects evolved from the heterostructures to ensure a fast electron transfer required in superb nonenzymatic glucose sensors will continue to face significant challenges.

In this research article, we chose the Cu NW as a primary nanobuilding block and demonstrate successful synthesis of hierarchical branching Cu@Cu_2O coaxial NWs with gram-scale by combining a facile hydrothermal route and subsequent control oxidation under mild conditions. The heterostructure obtained here is made by two-dimensional (2D) nanosheets (NSs) and 1D Cu NWs, wherein Cu core serves as built-in conduction channels for rapid electronic transport as well as structural reinforcement to overcome the mechanical rupture, and Cu_2O shell acts as the electron-transfer medium to process the detection of glucose. The detailed crystallographic analysis displayed both the interior core−shell heterostructure and external NSs located on the surface of the NW backbone are continuously grown from the crystallographic planes of the NW core material, resulting in well-defined junction with minimized lattice fringe distortion. This is highly desirable for the improvement of the charge transfer efficiency. To further demonstrate the function from such 3D nanostructures, we assembled the as-prepared branched NWs as powerful electrode in glucose sensor (Scheme 1) to prove the superior performance in term of sensitivity, precise specificity, and fast response characteristics.

2. EXPERIMENTAL SECTION

2.1. Chemical Reagents. Copper sulfate pentahydrate ($CuSO_4.5H_2O$), sodium hydroxide (NaOH, 99% purity), ethylenediamine (EDA), hydrazine (N_2H_4), ethanol, glucose, NaCl, acetaminophen, uric acid, and ascorbic acid, Nafion, sucrose, maltose, and fructose were purchased from a commercial source (Sigma-Aldrich). All solutions were prepared with ultrapure water (ca. 18 MΩ cm at 25 °C) from a Milli-Q integral water purification system.

2.2. Synthesis of Cu@Cu_2O NS-NWs. The formation of Cu@Cu_2O NS-NWs is based on the success in fabrication of pure metallic Cu NWs. In general synthesis, 250 mL of aqueous solution containing 1.7 mM $CuSO_4.5H_2O$, 2.2 M NaOH, 0.06 M EDA, and 4.4 mM N_2H_4 (molar ratio 1:1294:37:2.6) was placed in a 400 mL conical flask and heated at 80 °C in an oil-bath for 1 h. The reaction system is connected to the nitrogen-pressure assembly and mechanically stirred (500 rpm) throughout the whole process. The successful generation of Cu NWs can be declared by the solution color transformation from dark blue to red brown. Then the Cu@Cu_2O hierarchical structures were prepared by subsequent two-step air exposure treatments on the pregrown NWs, including (1) 55 min dry air exposure and (2) 155 min wet air exposure. Specifically, we first placed the pregrown NWs inside the furnace with purified arid air gas continuously flowing at the rate of 5 sccm. Meanwhile, the temperature was elevated up to 60 °C. An hour later, second wet air exposure was initiated uninterruptedly by introducing the flow of aqueous vapor until the humidity stabilized around 70%, whereas other conditions kept unchanged. The above process could also be readily applied to extend the preparation of high quality branched nanowires in large scale (see the Supporting Information, Figure S1). After the final exposure step, the product was dispersed in 10 mL of methanol. This suspension is then spin-coated (2000 rpm for 40 s) onto glass microscope slides (diameter 3 mm) until a uniform membrane is achieved.

2.3. Preparation of Cu@Cu_2O NS-NW Electrodes. Glassy carbon electrode (GCE, diameter 3 mm) was first burnished with 1 and 0.05 μm alumina suspensions, respectively, and followed by ultrasonic cleaning in ethanol and DI water before the start of the experiment. The Cu@Cu_2O NS-NW mesh was then transferred on the surface of polished GCE with a consequent cover Nafion film. The as-modified electrode is named as Nafion/Cu@Cu_2O NS-NWs/GCE. Nafion-coated GCE (i.e., Nafion/GCE) and Cu NWs modified electrode (i.e., Nafion/Cu NWs/GCE) were also assembled as counterpart.

DOI: 10.1021/acsami.5b04614
ACS Appl. Mater. Interfaces 2015, 7, 16802−16812

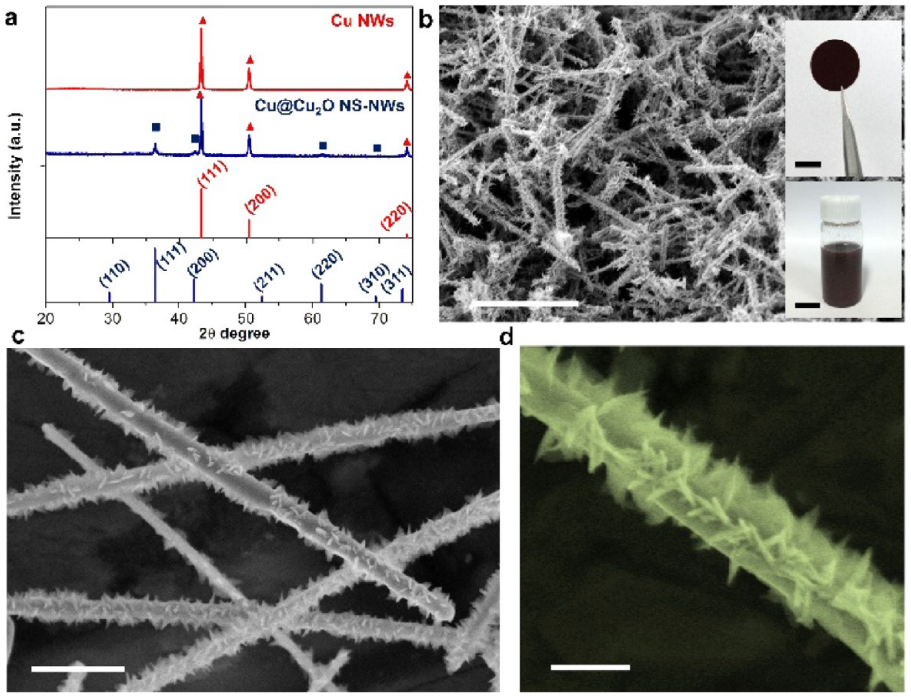

Figure 1. (a) XRD patterns of pristine Cu NWs (red) and the as obtained Cu@Cu_2O branched nanostructures (blue). The vertical red and blue lines signify the standard XRD patterns of face centered cubic Cu (JCPDS: 85−1326) and cubic Cu_2O (JCPDS: 05−0667), respectively. (b) Overview of as prepared products, scale bar, 1 μm. Top right inset is mesh pad composed of branched NWs, scale bar 3 mm. Bottom right inset is branched NW ink in methanol solvent with concentration of 5 mg/mL, scale bar 2 cm. (c) Typical SEM image shows multiple branches spread out from each backbone NW, scale bar 500 nm. (d) Observation of the individual branched structure at high-magnification, scale bar 100 nm.

2.4. Materials Characterizaion and Electrochemical Tests. The crystalline structure and morphology of the as-obtained nanoheterostructures were characterized by high resolution transmission electron microscope (HRTEM, JEOL, 200 kV) and scanning electron microscope (FEI.Co Sirion-200), respectively. X-ray powder diffraction (XRD) patterns were recorded by using Cu Kα irradiation (λ = 1.5406 Å) on a PAN alytical D/max-IIIA diffractometer. Cyclic voltammetric (CV) and amperometric (i−t) measurements were operated by using CHI 660D potentiostats (CH Instruments, USA) and PARSTAT4000 (AMETEK, Inc.) respectively. The reference and the counter electrodes adopted in tests are Ag/AgCl (3 M KCl) electrode and Pt wire, respectively. And the electrolyte adopted in this study is NaOH solution with an appropriate concentration. It is worth noting that the current response should be normalized to the geometric area of the working electrode for achieving more accurate results.

3. RESULTS AND DISCUSSION

3.1. Morphological and Structural Illustration. The holistic phase purity and crystal structure information on the two as-prepared samples, i.e., pristine Cu NWs and hierarchical Cu@Cu_2O NS-NWs, are provided in XRD patterns (see Figure 1a). All of the prominent diffraction peaks in both patterns can be precisely indexed to the face-centered cubic (fcc) Cu (JCPDS card no. 85−1326, $Fm\bar{3}m$, $a_0 = b_0 = c_0$ = 3.615 Å) and cubic phase Cu_2O (JCPDS card no. 05−0667, $Pn\bar{3}m$, $a_0 = b_0 = c_0$ = 4.269 Å). Peak broadening can also be detected which is attributed to nanocrystallinity induced small-size effects. Figure 1b reveals a typical SEM image of the as obtained branched nanostructured products, where the 1D structure with a distinct rough surface could be addressed. The corresponding magnified SEM images of the product (Figure 1c, d) manifest the structural details in further. The diameters of the as-obtained branched nanowires are typically in the range of 80−120 nm and their lengths are greater than 5 μm. Significantly, the products are also observed to exhibit hierarchical structures with multiple rows of 6−10 nm thick and 30−50 nm long 2D secondary NSs decorated on the major NW backbones. In addition, Figure 1d also exhibits that the angle between the NSs preferred orientations and the axis of the NW stem is approximately 90°. This observation verifies that these NSs possess an explicit epitaxial relation of crystalline structure to the backbone, which was also examined and confirmed by transmission electron microscope (TEM) illustration.

Further detailed structural analysis of the as-obtained NS-NWs was carried out by using a 200 kV TEM. Figure 2a reveals that the NWs backbone have uniform diameter throughout the length and the NSs densely and uniformly cover the surface of the NWs. Close inspection of a NS-NW (Figure 2b) shows that these on-wire NSs possess a thorn shape with length of ca. 40 nm and diameter nearby 20 nm. The selected area electron diffraction (SAED) in Figure 2b illustrates the single-crystalline nature of the nanostructure in spite of accompanied extra Cu_2O diffraction spots. Based on the SAED pattern, the as-obtained branched core−shell nanowire could be demonstrated as [110] preferred grown crystal. Unlike 5-fold twinned Cu NWs,[33] there are no reflections from multiple zone axes. Beside the spots from Cu core, it is noteworthy that Cu_2O (220) diffraction spot was also observed as coexist part with Cu (220). It apparently indicated that the thin layer (shell) epitaxial growth of Cu_2O happened on the surface of metallic Cu core within a range of critical thickness. To give definite element compositions and quantitative analysis of Cu and O throughout the heterostructures, EDS (energy disperse spectroscopy) point scanning (Figure 2c) on three different regions specified in Figure 2b was further operated. In the region (1), Cu signals are strong while the O signal intensity is negligible.

DOI: 10.1021/acsami.5b04614
ACS Appl. Mater. Interfaces 2015, 7, 16802−16812

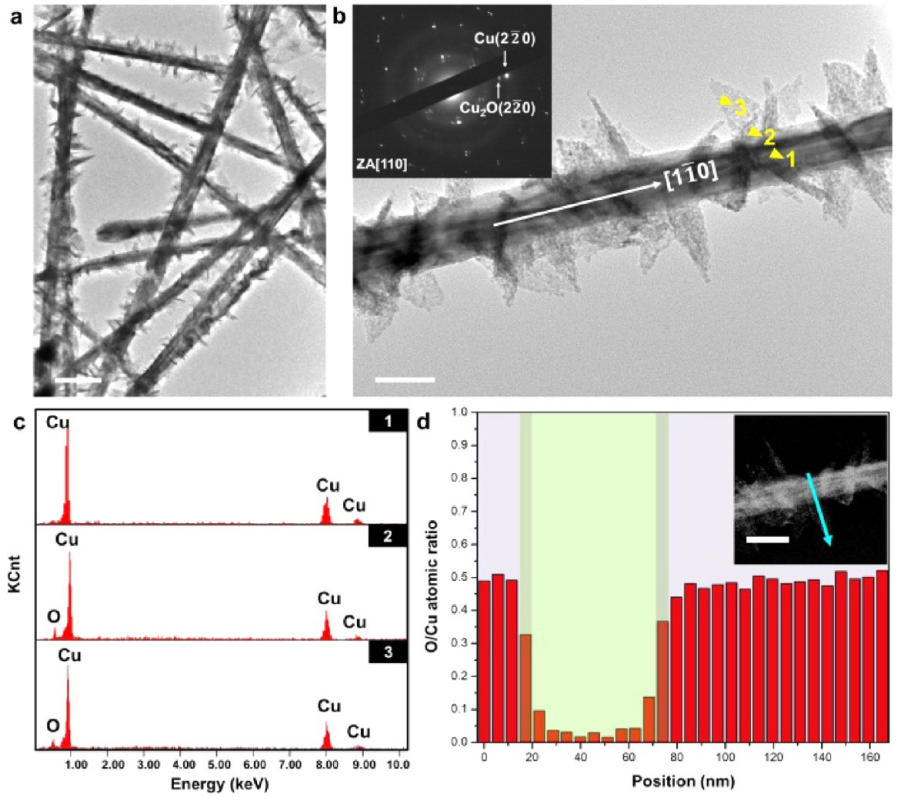

Figure 2. (a) TEM image of the branched nanowires, scale bar, 500 nm. (b) TEM image of branched NW with thorn shaped NS, scale bar, 100 nm. Inset is SAED taken from the center of the NW showing single-crystalline nature. (c) EDS point scanning data from the (1) NW backbone, (2) NW-NS junction, and (3) NS areas of the nanostructure labeled in panel b. (d) Cu/O atomic ratio profile extracted on the same NW across the junction, backbone, and branch regions. Inset is a corresponding STEM image of NW, scale bar 50 nm.

The stoichiometric ratio of Cu is above 99%. Moreover, energy spectra detected on the other selected spot areas along the NW backbone are also largely consistent. The EDS from region (2) indicates the appearance of Cu_xO_{1-x} ($x \approx 0.7$) state as a result of the interdiffusion of Cu and O. In the branch region (3), stoichiometric ratio of Cu and O was observed to be approximately 2.1 (at % Cu = 67.6; at % O=32.4). The relative chemical composition profile of Cu and O conducted as a function of distance is displayed in Figure 2d (induced by light blue arrow of inset). The O/Cu stoichiometric ratio first held steady at approximately 0.5:1 in the branch region involving the surface layer of NW backbone (first 18 nm and last 86 nm regions), then gradually decreased to around 0:1 toward the central region. This result suggests that such branched NWs may also be constructed by core−shell structure, with various certain levels of interdiffusion of Cu and O.

To find out the structure evolution and get further understanding of the crystal correlation between the NS branches and the NW backbone, we performed high-resolution TEM (HRTEM) investigation on some tiny branched part (region α, β) and their adjacent area (γ) specified in Figure 3a. The lattice-resolved HRTEM image (Figure 3b) clearly suggests that entire branch region (α1) is single crystalline without any apparent structural flaws, and moreover, such crystallographic structure continues into the structure interface (α2) and backbone (α3). The lattice spacing of 0.258 nm in backbone regions and 0.301 nm within the branch inosculate well with (1$\bar{1}$0) interplanar spacing of fcc Cu and cubic Cu_2O, respectively. FFT (fast Fourier transform) on selected dotted yellow boxes as designated in the HRTEM image (i.e., region α1, α2, and α3) we performed all give identical reciprocal lattice points (inset of Figure 3b). These typical FFT results manifest the parallel relationship between (1$\bar{1}$0) Cu_2O and (1$\bar{1}$0) Cu planes, implying that the Cu_2O NS branch may grow epitaxial from the crystallographic planes of the Cu backbone. The FFT patterns also confirm the basal plane of the NS is (00$\bar{2}$). This observation is in accordance with observed 90° angle between the NS and the NW. At the HRTEM image in both Figure 3c, d, distinct interface can be typically observed between the outer layers (bright part) and core of backbone (dark part), wherein two different but parallel lattice planes with 0.258 and 0.301 nm distances can be assigned to the (1$\bar{1}$0) planes of Cu and Cu_2O separately. Besides, the (00$\bar{2}$) planes of Cu_2O NS can also be observed to stack parallel to the (00$\bar{2}$) ones of Cu NW core at these regions. These lattice fringes nicely stretched from the NW unto the local thin crystalline shell, which is again consist to the scene at the heterojunction as we discussed above, coincides with our suppose for the epitaxial growth of Cu_2O NSs.

The Moiré patterns, an interference pattern created by two overlaid gratings with different periodicities/orientations,[34] is another intriguing feature observed among the HRTEM investigation as seen in Figure 3d, e. Here the Moiré patterns were generated through the mutual overlaps of the crystalline Cu_2O and Cu lattice. Figure 3e, an enlarged inverse reconstructed HRTEM image of the white square area in Figure 3d, illustrates the parallel relations between Moiré fringes and {2$\bar{2}$0} Cu planes and it can also be found that every Moiré fringes embodies 6 Cu (2$\bar{2}$0) fringes. Accordingly, we could calculate the Cu_2O (2$\bar{2}$0) (d_2) interplanar spacing to be 1.488 Å by substituting n = 6 and the lattice spacing of Cu

DOI: 10.1021/acsami.5b04614
ACS Appl. Mater. Interfaces 2015, 7, 16802−16812

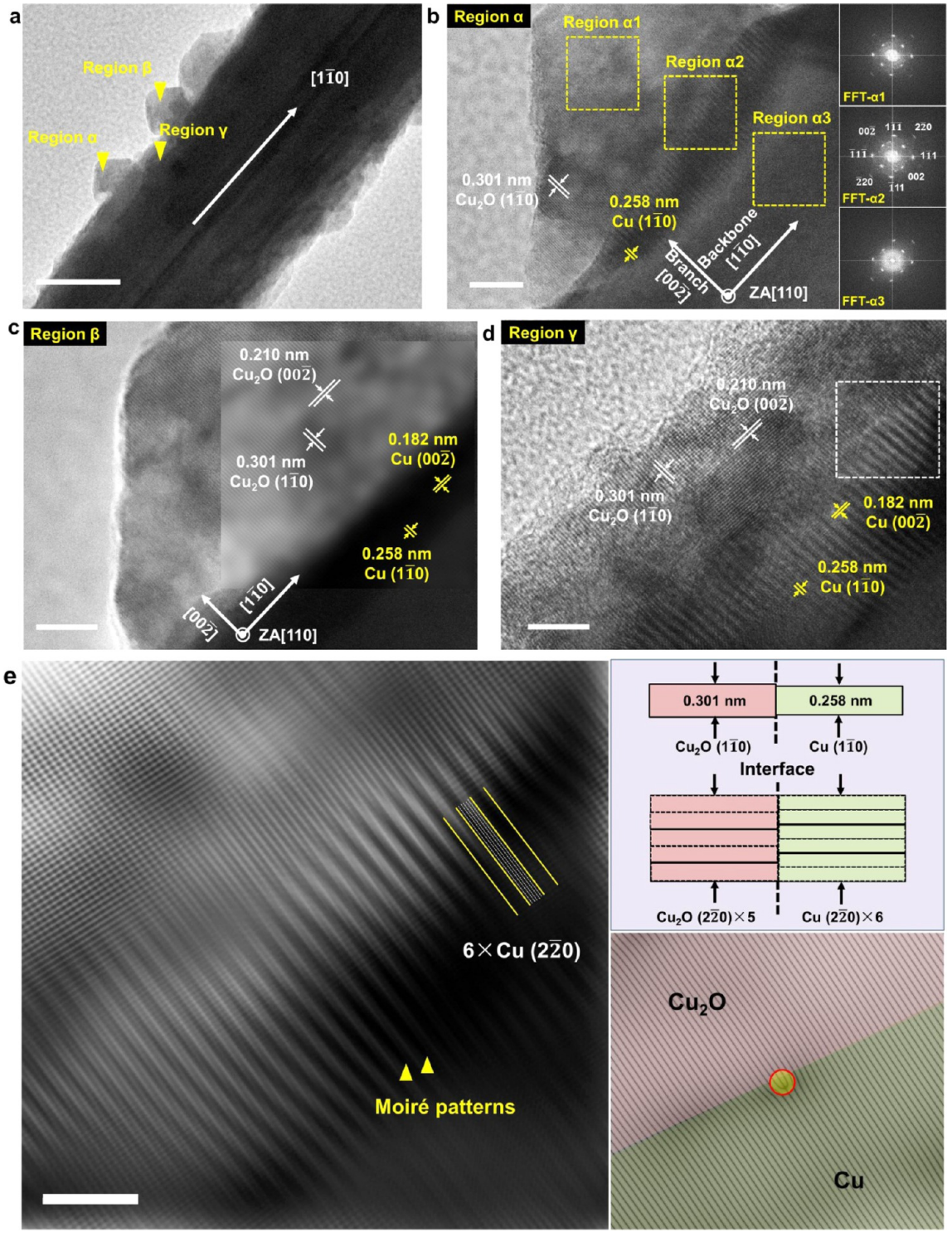

Figure 3. (a) TEM image of a typical branched coaxial NW, revealing the constant angle of approximately 90° between the branched parts and the NW axis. Scale bar, 50 nm. (b) Corresponding HRTEM images of the region α in panel a), scale bar, 5 nm. FFT was further performed in three yellow dashed boxes and exhibits identical patterns as shown in the inset. (c) Close inspection of region β, scale bar, 5 nm. Inset is superimposed inverse reconstructed image at the junction area. (d) High-resolution TEM image of selected area γ at the heterojunction, scale bar, 5 nm. (e) Inverse reconstructed TEM image of the heterojunction interface as marked by dashed white box in panel d, which demonstrates distinct Moiré patterns. Top right inset is schematics of the interface of the $(1\bar{1}0)_{Cu}$ plane and the $(1\bar{1}0)_{Cu2O}$ plane and bottom right inset is corresponding inversed FFT image along the $[1\bar{1}0]$ orientation. The typical lattice fringe distortion at the core−shell interface is emphasized by the red-circled light-yellow area, scale bar 1 nm.

$(2\bar{2}0)$ (d_1 = 1.275 Å) into Moiré repeat formula $n = d_1/(d_2 - d_1)$, $d_2 > d_1$.[35] Thus, a lattice constant of $a(Cu_2O)$ = 4.207 Å could be further derived. In addition, the number of Cu_2O $(2\bar{2}0)$ planes in a Moiré repeat could also be figured out by nd_1/d_2, which is 5. It means that every five $(2\bar{2}0)$ planes in the Cu_2O shell could match six $(2\bar{2}0)$ planes of the Cu NW

DOI: 10.1021/acsami.5b04614
ACS Appl. Mater. Interfaces 2015, 7, 16802−16812

core, experiencing a remarkable attenuation of dislocation density with lattice misfit of 2.6% (top right inset of Figure 3e). This is much smaller than the natural lattice misfit between Cu and Cu2O (15.3%, calculated by $f = (a\mathrm{Cu_2O}\text{-}a\mathrm{Cu})/a\mathrm{Cu_2O}$). Correspondingly, in bottom right inset of Figure 3e, the selected inverse FFT image shows that bare distortion (less than 5%) could be observed at the heterostructure interface in the marked area and most of the lattice fringes span smoothly through the junction interface. These findings demonstrate that epitaxial oxide growth will accommodate interfacial lattice strain in a local minimum energy state to form a well-defined heterojunction with low defect density. This intimate contact would enable excellent charge transition with minimal electron restrain at the interface, which can be utilized in the application of efficient sensors.

3.2. Function as Glucose Detection Electrode. The successful synthesis of the Cu@Cu_2O NS-NW heterostructure offers an excellent electrode candidate for nonenzymatic glucose sensor. The primary Cu NW core combined with the well-defined Cu/Cu_2O heteroepitaxial junction provides short path lengths for electronic delivery to facilitate preeminent sensitivity. The on-wire NSs offer sufficient specific surface area and alleviate the aggregation of NWs, assuring more active sites for easier permeation of the liquid electrolyte. To identify its performance for detection of glucose, we employed such heterostructured NS-NWs as anode material to decorate glassy carbon electrode (GCE) surface. As a reference, we also include the Cu NWs without hierarchical NSs in the corresponding tests to prove superior of the as-proposed structures.

The cyclic voltammograms (CVs) of the modified Nafion/Cu@Cu_2O NS-NW/GCE electrode and the bare Nafion/GCE electrode were conducted in 50 mM NaOH solution at a scan rate of 10 mV s^{-1} in the presence and absence of glucose, respectively. As shown in Figure 4a, Nafion/GCE electrodes exhibited no obvious redox peak in 50 mM NaOH solution and inappreciable current increase after the addition of glucose, indicating that the bare electrode is electrochemically inactive for glucose oxidation. In contrast, six well-demarcated reversible redox peaks can be distinctly observed on the Nafion/Cu@Cu_2O NS-NW/GCE electrode before the addition of glucose (blue trace). This is assigned to the well-known electrochemical process involving the multistep reversible transition of Cu(0)/Cu(I), Cu(0)/Cu(II) accompanied by Cu(I)/Cu(II), and Cu(II)/Cu(III) in an alkaline system under the specified potential region according to the previous research[36,37]

$$\mathrm{Cu_2O} + 2\mathrm{OH^-} \rightarrow 2\mathrm{CuO} + \mathrm{H_2O} + 2\mathrm{e}- \quad (1)$$

$$\mathrm{CuO} + \mathrm{OH^-} \rightarrow \mathrm{CuOOH} + \mathrm{e^-CuO} + \mathrm{OH^-} + \text{gluconic acid} \quad (2)$$

However, in the presence of 2 mM glucose, the CV profile (red trace) shows that the broad peak 3 at 0.27 V (vs Ag/AgCl), which is most considered to be correlated with the generation of Cu(III) species from the Cu(II) solid(s) and hydroxide ions, has almost disappeared and been replaced by a clear shoulder peak at 0.65 V during the anodic scan. The differences can be solely ascribed to the oxidation of glucose on the Cu@Cu_2O NS- NW modified GCE assisted by the Cu(II)/Cu(III) redox couple on the basis of earlier works.[37,38] Evidently, after the initial conversion from Cu(0) and Cu(I) to Cu(II) on a Cu@Cu_2O electrode during CV measurement (peak 2), Cu(II) should be subsequently oxidized to Cu(III) state. But, in an alkaline medium, the isomerized intermediate of injected glucose is immediately isomerized to an enediol form via deprotonation process, and this intermediate will be gradually oxidized to gluconolactone and further hydrolyzed to gluconic acid by Cu(III), resulting in disappearance of peak 3 and emerging of glucose oxidation peak near the positive potential range end. Herein, the Cu(III) species are proposed to play the role as an electron transport medium to catalyze glucose oxidation. In addition, the inspection of oxygen-independent behavior of such electrochemical processes is also carried out, as shown in Figure S2 in the Supporting Information. The result demonstrates that there is no significant changes between CVs with or without glucose when removing oxygen from the system. Thus, such an enhanced catalytic current response at a potential range of 0.20−0.80 V in particular, depending on whether the glucose exists or not, provides the basis for the utilization of our modified electrode in glucose sensing.

Before amperometric detection of glucose, we optimized possible experimental parameters that may affect the analytical performance of the fabricated nonenzymatic sensor involving scan rate, concentrations of glucose and NaOH, applied potential, and NS-NWs loading amount. As shown in Figure 4b, the CV measurements of modified electrode were performed at different scan rates of 10−700 mV s^{-1}. The comparative profiles show that the redox peak currents changed linearly and excellent correlation coefficients are determined, indicating the kinetic surface adsorption/diffusion dominant electro-oxidation of glucose on Nafion/Cu@Cu_2O NS-NWs/GCE. Figure 4c presents the performance of the sensor in 50 mM NaOH solution under different glucose concentration from 0 to 10 mM. As desired, both of anodic shift of the peak potential and dramatic enhancement of the oxidative peak current are observed. However, a cathodic potential shift does not appear and the peak current has only a slightly increase. This indicates a nonreversible electrochemical oxidation process. In contrast (inset of Figure 4c), on the Nafion/GCE electrode, there is no evident current increase before and after adding glucose with concentration of 10 mM under the same constraints. Besides, owing to the largely formed hydroxyl radical at high applied potential, the anodic current could also increase significantly with the elevating of NaOH concentration (Figure 4d). However, any further increase in the electrolyte concentration does not yield a proportional rise of the current (Figure S3), in fact, the loading of NS-NWs on the GCE is not infinite but limited. Thus, we choose 50 mM NaOH as ultimately selected alkaline electrolyte for subsequent tests. To establish the preferable potential for real time electroactivity study through a typical $i-t$ technique, various potentials in the range of 0.3−0.7 V are examined in amperometric measurements, wherein successive glucose injection concentration is 2 mM, as presented in Figure 4e. It can be clearly seen that the current response showed an overall trend of rise over a span of 0.3−0.6 V and, when the applied potential exceed 0.6 V no visible current change experienced but the noise signals grew more severe, leading to disturbance of oxidative current response (see detail in Figure S4). Therefore, in the follow-up experiments, 0.6 V is adopted as the optimum potential. Moreover, Figure 4f presents the influence of the Cu@Cu_2O NS-NWs loading amount on the current response of the electrode to 2 mM glucose. On the one hand, increasing loading capacity initially increased the response. This is attributed to increased active adsorption sites. On the other hand, the currents were decreased gradually when the loading amount is greater than 10 mg/mL, mainly because of the

DOI: 10.1021/acsami.5b04614
ACS Appl. Mater. Interfaces 2015, 7, 16802−16812

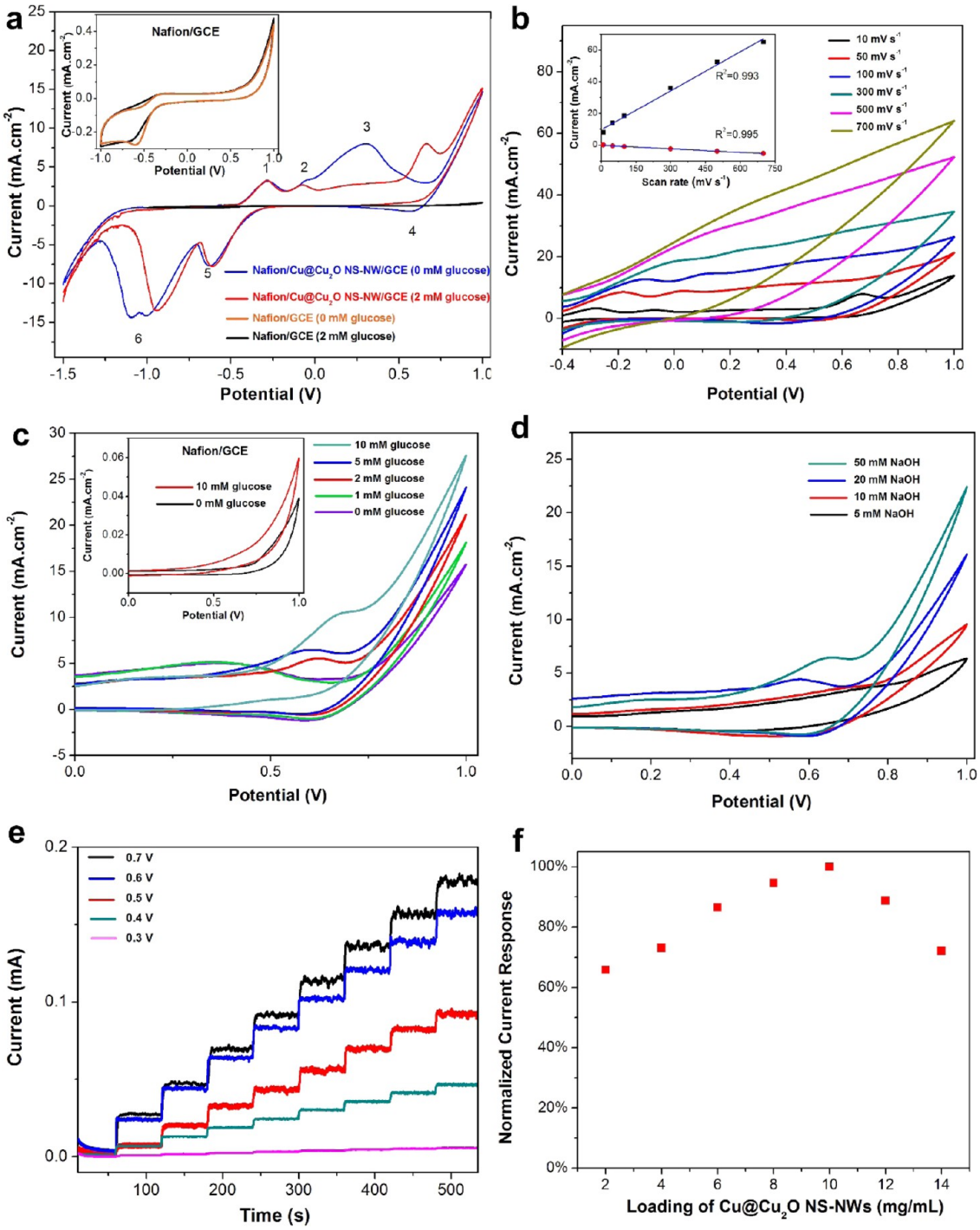

Figure 4. (a) CV curves of the Nafion/Cu@Cu_2O NS-NWs/GCE and bare Nafion/GCE in the absence and presence of 2 mM glucose. The concentration of NaOH electrolyte is 50 mM, and scan rate is 10 mV s^{-1}; the inset show magnified scan curves from the Nafion/GCE. (b) CVs of Cu@Cu_2O NS-NW-modified GCE at scan rates varying from 10 to 700 mV s^{-1} in 50 mM NaOH solution containing 2 mM glucose. Inset shows plots of peak current as a function of scan rate and linearly fitted curves. (c) CVs of the Nafion/Cu@Cu_2O NS-NWs/GCE in the presence of glucose with different concentrations. Inset is Nafion/GCE control sample. The electrolyte is 50 mM NaOH, the scan rate is 10 mV s^{-1}. (d) CVs of the Nafion/Cu@Cu_2O NS-NWs/GCE with the appearance of 2 mM glucose under different concentrations of NaOH, the scan rate is 10 mV s^{-1}. (e) Real time current response of Nafion/Cu@Cu_2O NS-NWs/GCE at various potentials in the range of 0.3−0.7 V with successive additions of 50 mM glucose. (f) Normalized current response versus the loading of Cu@Cu_2O NS-NWs.

undesirable transport resistance in the deeper immobilized layer resulted by long electron pass distance.

In optimization conditions, amperometric responses in constantly stirred NaOH solutions to successive injection of glucose were recorded. As displayed in Figure 5a, b, amperometric currents toward Cu@Cu2O NS-NWs modified electrodes stage increased with the level of glucose and the response time is much smaller than 0.1 s (Figure 5b), demonstrating efficient catalytic electro-oxidation ability. Moreover, under the same glucose concentration, the current response of the Nafion/Cu@Cu_2O NS-NWs/GCE is much more significant than that of the Nafion/Cu NWs/GCE. Figure 5c shows the

DOI: 10.1021/acsami.5b04614
ACS Appl. Mater. Interfaces 2015, 7, 16802−16812

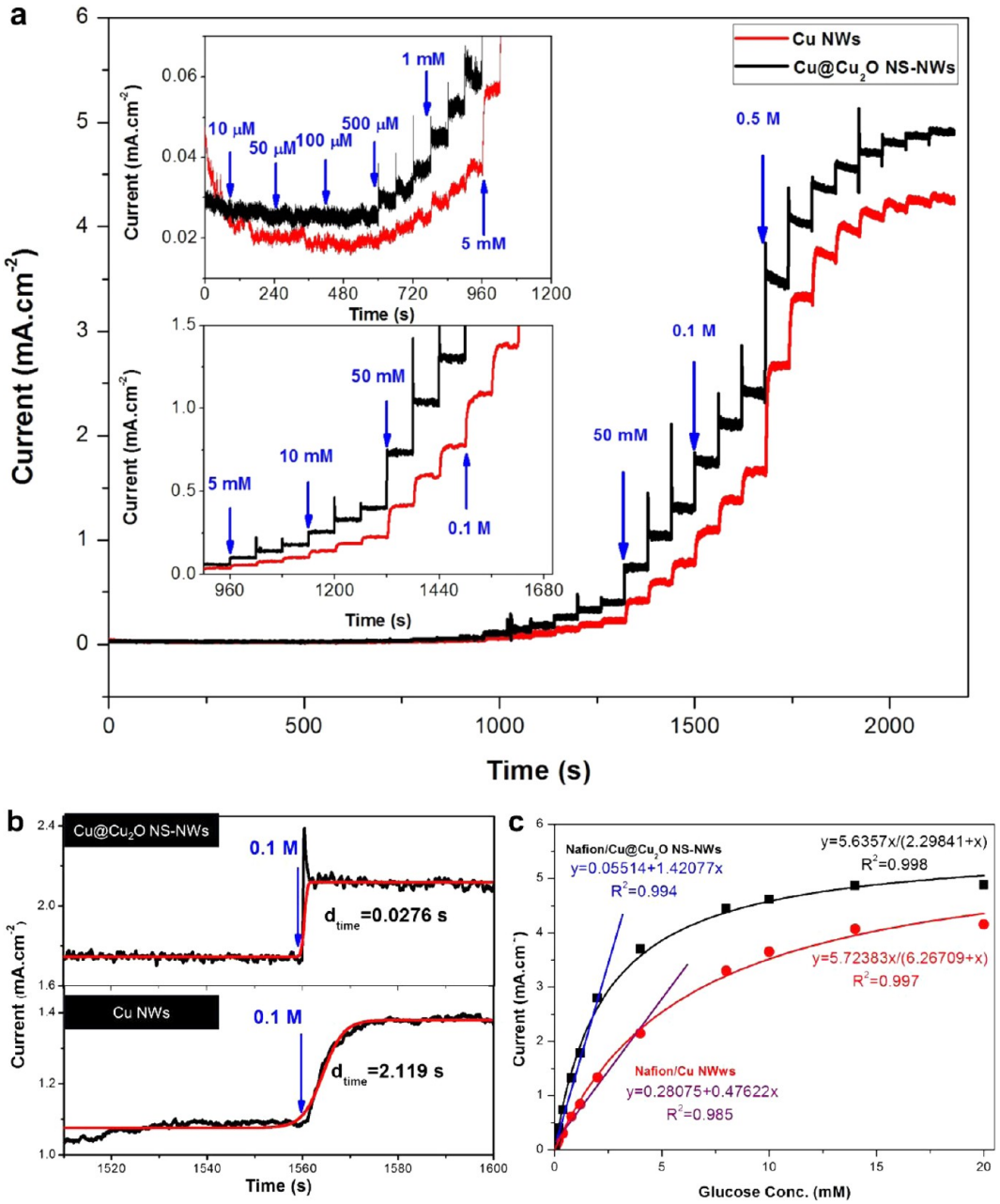

Figure 5. (a) Amperometric response of the Nafion/Cu@Cu_2O NS-NWs/GCE (black) and Nafion/Cu NWs/GCE (red) in 50 mM NaOH. The successive glucose addition is from 10 μM to 0.5 M and each concentration injected three times. The applied potential is 0.6 V. (b) Amperometric response to 0.1 M glucose. Exponential fittings with time constants of ca. 0.028 s and ca. 2.119 s for Cu@Cu_2O NS-NW- and Cu NW-modified electrode, respectively, are shown. c) The corresponding calibration curve.

corresponding linear dependence of current response versus different glucose concentrations. The sensitivity of the Nafion/Cu@Cu_2O NS-NWs/GCE (1420 $\mu A mM^{-1} cm^{-2}$) is almost 3-fold greater than that of the Nafion/Cu NWs/GCE (476 $\mu A\ mM^{-1}\ cm^{-2}$). Furthermore, the limit of detection (40 nM, S/N = 3) in Nafion/Cu@Cu_2O NS-NWs/GCE is lower than that of Nafion/Cu NWs/GCE (3.92 μM, S/N = 3), whereas the liner range (0.7 μM−2.0 mM) of Nafion/Cu@Cu_2O NS-NWs/GCE is narrower than Nafion/Cu NWs/GCE (3.9 μM−4 mM). Compared with other reported Cu-based or noble metal-based nanostructured nonenzymatic glucose sensors (see the Supporting Information, Table S1), the as-prepared Cu@Cu_2O NS-NWs electrode shows ultrahigh sensitivity, fast response, good high-concentration susceptibility and low detection limit. This benefit can be ascribed to the cooperative effects of: (1) large surface area from the hyperbranched nanostructure, (2) good tolerance to volumetric change benefited from adequate free space between neighboring branches, (3) favorable electronic transfer channels evolved from the high-quality heterojunction, and (4) enhanced conductivity inherited from the metallic copper NWs. All of these unique properties endow immobilized NS-NW network with perfect electrical conducting performance between the target molecules and glassy carbon substrate. However, it should be noted that the linear correlation between current and glucose concentration in this study works only in very small range below 2.0 mM, thus the formula $I = aC_{glucose}/(b + C_{glucose})$ based on Langmuir isothermal theory is further

DOI: 10.1021/acsami.5b04614
ACS Appl. Mater. Interfaces 2015, 7, 16802−16812

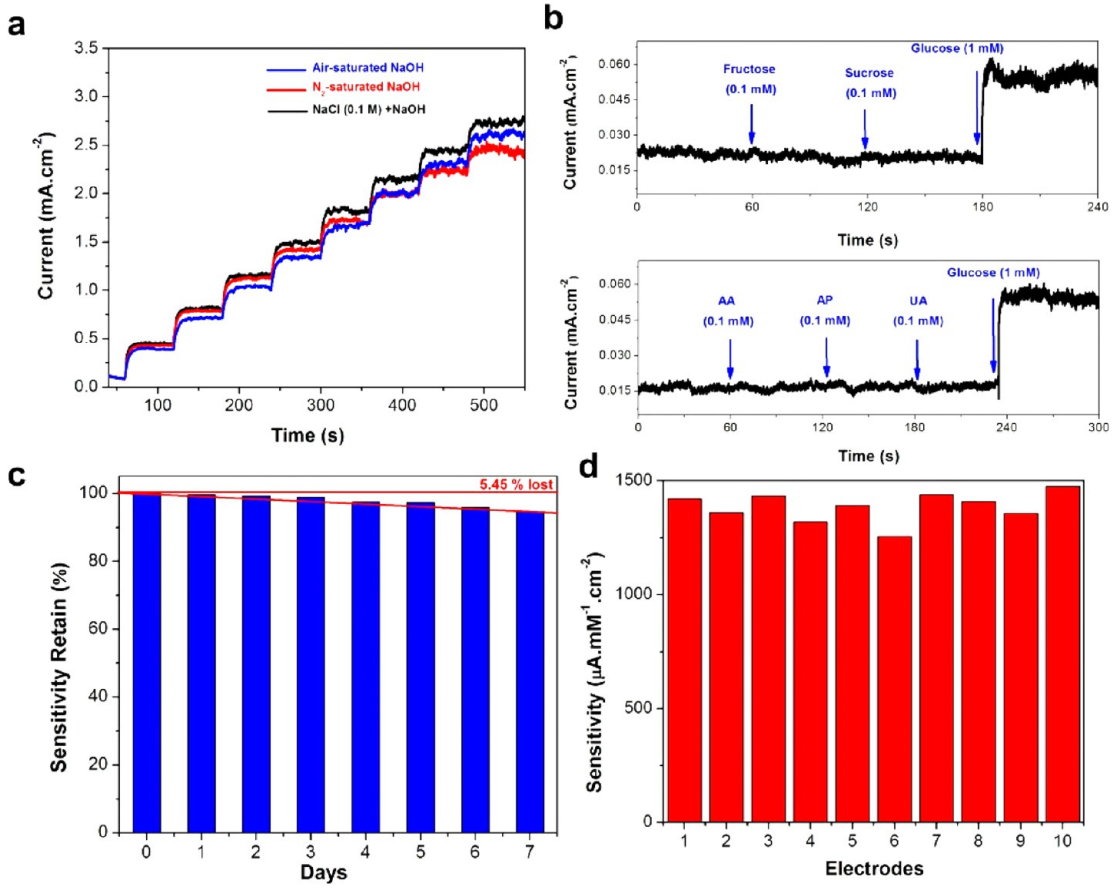

Figure 6. (a) Real time current response of the Nafion/Cu@Cu_2O NS-NWs/GCE to 50 mM glucose in air-saturated NaOH (blue), nitrogen-saturated NaOH (red), and air-saturated NaOH fortified with 0.1 M NaCl (black). The NaOH solution concentration is equally 50 mM. (b) Current response of the Nafion/Cu@Cu_2O NS-NWs/GCE upon successive addition of various interfering species with 0.1 mM concentration and 1 mM glucose in 50 mM NaOH at 0.6 V. (c) Normalized sensitivity of Nafion/Cu@Cu_2O NS-NWs/GCE toward glucose analysis by amperometric measurements every day over 1 week. (d) Comparison in the sensitivity of ten numbers of identically fabricated Nafion/Cu@Cu_2O NS-NWs/GCE analyzed in 50 mM NaOH at 0.6 V (vsAg/AgCl).

employed to achieve a wider dynamic range of coverage in real blood samples detection, where the normal glucose level is of 4−7 mM.[39,40] This gives $I = 5.6C_{glucose}/(2.3 + C_{glucose})$ for Cu@Cu_2O NS-NWs modified electrode as the fitting equation with R^2=0.998. In order to verify the reliability of as-obtained calibration curve, three additional independent real-time amperometric tests were also performed and nothing dramatically change is found for each data point, as illustrated in Figure S5. The result indicates excellent reproducibility.

To assess the broader practical feasibility of proposed Nafion/Cu@Cu_2O NS-NWs/GCE, especially in physiological fluids such as human blood, its recognition capability of glucose from interfering substances include dissolved O_2, and Cl^- has also been inspected with multiple chronoamperometry measurements. As shown in Figure 6a, neither oxygen exhausting nor the existence of Cl^- have effect on the glucose sensing performance, which clearly ascertains favorable anti-interference ability against Cl- and oxygen-independent peculiarity. In addition, we further evaluated the glucose specific selectivity of such developed electrode among some frequently concomitant sugars like sucrose, fructose and endogenous reducing compounds such as ascorbic acid (AA), uric acid (UA), acetaminophen (AP). Figure 6b demonstrates that the current signals generated by high concentration of these interfering species are trivial compared with that after 1 mM glucose injection into 50 mM NaOH at 0.6 V, indicating the proposed sensor is very fit for glucose detection. The long-term stability is another great importance for practical applications. In this work, the proposed sensor based on Cu@Cu_2O NS-NWs modified electrode was stored in ambient environment and its sensitivity was evaluated once a day for 1 week through amperometric response. The result collected from the repeated experiments (Figure 6c) revealed that the self-made sensor could retain 94.55% of the incipient sensitivity, implying the exceptional stability for longer duration applications. Additionally, parallel chronoamperometric inspections of 10 identically fabricated electrodes was evaluated to ascertain its reproducibility. As illustrated in Figure 6d, the sensitivity comparative histograms exhibit relative standard deviations (RSD) of only 4.7%. Such favorable reproducibility confirms the high structural stability of our designed architecture during electrooxidation of glucose. We performed human blood glucose monitoring by using prepared sensor and compared the results with data collected from OneTouch Verio IQ glucometer to check the practicability. According to a contrast and analysis (Table S2), it can be found that the results obtained through commercial standard tool and fabricated enzymeless sensor have few discrepancies, demonstrating its great potential for satisfying the needs of glucose determination in real production and livelihood with sufficient accuracy.

DOI: 10.1021/acsami.5b04614
ACS Appl. Mater. Interfaces 2015, 7, 16802−16812

4. CONCLUSION

In summary, we have presented an efficient and convenient strategy for the growth of hierarchical branching Cu@Cu_2O NWs. The uniqueness of the structure is that, the Cu NW core is coated with Cu_2O interlayer shell including branched 2D NSs epitaxially growing on 1D NWs surface. The investigation on the structure evolution of such NS-NWs indicated that the growth of branches is governed by lattice mismatch derived from heterogeneous engagement at the interface. These Cu@Cu_2O NS-NWs remarkably enhanced glucose sensing performance in terms of sensitivity, linear range, response rate, selectivity and stability as well as reproducibility. The improvement is mainly promoted by a cooperative effect between NW backbone and secondary on-wire branches as well as the less-defective heterogeneous junctions. We believe the design structure here may potentially be expanded to other metal oxide anode material system for electrochemical analysis.

■ ASSOCIATED CONTENT

Supporting Information

The Supporting Information is available free of charge on the ACS Publications website at DOI: 10.1021/acsami.5b04614.

Digital photo of Cu@Cu2O branched NWs production, additional electrochemical measurements, comparison between Cu@Cu2O NS-NWs modified electrode and reported materials, and glucose detection in real human blood samples (PDF)

■ AUTHOR INFORMATION

Corresponding Authors

*E-mail: ziyanghuo@gmail.com.
*E-mail: zfyancat@upc.edu.cn.

Notes

The authors declare no competing financial interest.

■ ACKNOWLEDGMENTS

We thank Prof. Zhiping (Gordon) Xu and Prof. Ming Bo for their guidance and help in experiments, respectively. This work has been financially supported by the Key Joint Foundation of PetroChina, Natural Science Foundation of China (NSFC U1362202, 51271215, 21106185), PetroChina key programs on oil refinery catalysts (2010E-1908, 2010E-1903), and Fundamental Research Funds for Central Universities (15CX02069A).

■ REFERENCES

(1) Wang, J. Electrochemical Glucose Biosensors. *Chem. Rev.* **2007**, *108*, 814−825.
(2) Heller, A.; Feldman, B. Electrochemical Glucose Sensors and Their Applications in Diabetes Management. *Chem. Rev.* **2008**, *108*, 2482−2505.
(3) Clark, L. C.; Lyons, C. Electrode Systems for Continuous Monitoring in Cardiovascular Surgery. *Ann. N. Y. Acad. Sci.* **1962**, *102*, 29−45.
(4) Newman, J. D.; Turner, A. P. F. Home Blood Glucose Biosensors: A Commercial Perspective. *Biosens. Bioelectron.* **2005**, *20*, 2435−2453.
(5) Hrapovic, S.; Liu, Y.; Male, K. B.; Luong, J. H. T. Electrochemical Biosensing Platforms Using Platinum Nanoparticles and Carbon Nanotubes. *Anal. Chem.* **2003**, *76*, 1083−1088.
(6) Song, Y.; Qu, K.; Zhao, C.; Ren, J.; Qu, X. Graphene Oxide: Intrinsic Peroxidase Catalytic Activity and Its Application to Glucose Detection. *Adv. Mater.* **2010**, *22*, 2206−2210.
(7) Park, S.; Chung, T. D.; Kim, H. C. Nonenzymatic Glucose Detection Using Mesoporous Platinum. *Anal. Chem.* **2003**, *75*, 3046−3049.
(8) Yuan, J. H.; Wang, K.; Xia, X. H. Highly Ordered Platinum-Nanotubule Arrays for Amperometric Glucose Sensing. *Adv. Funct. Mater.* **2005**, *15*, 803−809.
(9) Doménech, A.; Alarcón, J. Microheterogeneous Electrocatalytic Chiral Recognition at Monoclinic Vanadium-Doped Zirconias: Enantioselective Detection of Glucose. *Anal. Chem.* **2007**, *79*, 6742−6751.
(10) Lu, J.; Do, I.; Drzal, L. T.; Worden, R. M.; Lee, I. Nanometal-Decorated Exfoliated Graphite Nanoplatelet Based Glucose Biosensors with High Sensitivity and Fast Response. *ACS Nano* **2008**, *2*, 1825−1832.
(11) Ahmad, R.; Vaseem, M.; Tripathy, N.; Hahn, Y.-B. Wide Linear-Range Detecting Nonenzymatic Glucose Biosensor Based on CuO Nanoparticles Inkjet-Printed on Electrodes. *Anal. Chem.* **2013**, *85*, 10448−10454.
(12) Guo, C.; Huo, H.; Han, X.; Xu, C.; Li, H. Ni/CdS Bifunctional Ti@TiO_2 Core−Shell Nanowire Electrode for High-Performance Nonenzymatic Glucose Sensing. *Anal. Chem.* **2013**, *86*, 876−883.
(13) Niu, X.; Lan, M.; Zhao, H.; Chen, C. Highly Sensitive and Selective Nonenzymatic Detection of Glucose Using Three-Dimensional Porous Nickel Nanostructures. *Anal. Chem.* **2013**, *85*, 3561−3569.
(14) Song, J.; Xu, L.; Zhou, C.; Xing, R.; Dai, Q.; Liu, D.; Song, H. Synthesis of Graphene Oxide Based CuO Nanoparticles Composite Electrode for Highly Enhanced Nonenzymatic Glucose Detection. *ACS Appl. Mater. Interfaces* **2013**, *5*, 12928−12934.
(15) Bierman, M. J.; Jin, S. Potential Applications of Hierarchical Branching Nanowires in Solar Energy Conversion. *Energy Environ. Sci.* **2009**, *2*, 1050−1059.
(16) Wu, H.; Xu, M.; Wang, Y.; Zheng, G. Branched Co3O4/Fe2O3 Nanowires as High Capacity Lithium-ion Battery Anodes. *Nano Res.* **2013**, *6*, 167−173.
(17) Jiang, X.; Tian, B.; Xiang, J.; Qian, F.; Zheng, G.; Wang, H.; Mai, L.; Lieber, C. M. Rational Growth of Branched Nanowire Heterostructures with Synthetically Encoded Properties and Function. *Proc. Natl. Acad. Sci. U. S. A.* **2011**, *108*, 12212−12216.
(18) Jung, Y.; Ko, D.-K.; Agarwal, R. Synthesis and Structural Characterization of Single-Crystalline Branched Nanowire Heterostructures. *Nano Lett.* **2006**, *7*, 264−268.
(19) Zhao, Y.; Zhang, Y.; Zhao, H.; Li, X.; Li, Y.; Wen, L.; Yan, Z.; Huo, Z. Epitaxial growth of hyperbranched Cu/Cu2O/CuO core-shell nanowire heterostructures for lithium-ion batteries. *Nano Res.* **2015**, 1−14.
(20) Cao, X.; Wang, N. A Novel Non-enzymatic Glucose Sensor Modified with Fe2O3 Nanowire Arrays. *Analyst* **2011**, *136*, 4241−4246.
(21) Zhu, C.; Guo, S.; Dong, S. PdM (M = Pt, Au) Bimetallic Alloy Nanowires with Enhanced Electrocatalytic Activity for Electrooxidation of Small Molecules. *Adv. Mater.* **2012**, *24*, 2326−2331.
(22) Pradhan, D.; Niroui, F.; Leung, K. T. High-Performance, Flexible Enzymatic Glucose Biosensor Based on ZnO Nanowires Supported on a Gold-Coated Polyester Substrate. *ACS Appl. Mater. Interfaces* **2010**, *2*, 2409−2412.
(23) Zhang, Y.; Su, L.; Manuzzi, D.; de los Monteros, H. V. E.; Jia, W.; Huo, D.; Hou, C.; Lei, Y. Ultrasensitive and Selective Non-enzymatic Glucose Detection Using Copper Nanowires. *Biosens. Bioelectron.* **2012**, *31*, 426−432.
(24) Dong, X.-C.; Xu, H.; Wang, X.-W.; Huang, Y.-X.; Chan-Park, M. B.; Zhang, H.; Wang, L.-H.; Huang, W.; Chen, P. 3D Graphene−Cobalt Oxide Electrode for High-Performance Supercapacitor and Enzymeless Glucose Detection. *ACS Nano* **2012**, *6*, 3206−3213.
(25) Shim, J. H.; Lee, Y.; Kang, M.; Lee, J.; Baik, J. M.; Lee, Y.; Lee, C.; Kim, M. H. Hierarchically Driven IrO2 Nanowire Electrocatalysts for Direct Sensing of Biomolecules. *Anal. Chem.* **2012**, *84*, 3827−3832.
(26) Xia, H.; Xiong, W.; Lim, C.; Yao, Q.; Wang, Y.; Xie, J. Hierarchical TiO2-B Nanowire@α-Fe2O3 Nanothorn Core-branch

DOI: 10.1021/acsami.5b04614
ACS Appl. Mater. Interfaces 2015, 7, 16802−16812

Arrays as Superior Electrodes for Lithium-ion Microbatteries. *Nano Res.* **2014**, *7*, 1797−1808.
(27) Shi, J.; Li, J.; Huang, X.; Tan, Y. Synthesis and Enhanced Photocatalytic Activity of Regularly Shaped Cu2O Nanowire Polyhedra. *Nano Res.* **2011**, *4*, 448−459.
(28) Zhou, W.; Cheng, C.; Liu, J.; Tay, Y. Y.; Jiang, J.; Jia, X.; Zhang, J.; Gong, H.; Hng, H. H.; Yu, T.; Fan, H. J. Epitaxial Growth of Branched α-Fe2O3/SnO2 Nano-Heterostructures with Improved Lithium-Ion Battery Performance. *Adv. Funct. Mater.* **2011**, *21*, 2439−2445.
(29) Liu, J.; Jiang, J.; Cheng, C.; Li, H.; Zhang, J.; Gong, H.; Fan, H. J. Co3O4 Nanowire@MnO2 Ultrathin Nanosheet Core/Shell Arrays: A New Class of High-Performance Pseudocapacitive Materials. *Adv. Mater.* **2011**, *23*, 2076−2081.
(30) Zhou, S.; Yang, X.; Lin, Y.; Xie, J.; Wang, D. A Nanonet-Enabled Li Ion Battery Cathode Material with High Power Rate, High Capacity, and Long Cycle Lifetime. *ACS Nano* **2011**, *6*, 919−924.
(31) Feng, Y.; Cho, I. S.; Rao, P. M.; Cai, L.; Zheng, X. Sol-Flame Synthesis: A General Strategy To Decorate Nanowires with Metal Oxide/Noble Metal Nanoparticles. *Nano Lett.* **2012**, *13*, 855−860.
(32) Xia, X.; Tu, J.; Zhang, Y.; Chen, J.; Wang, X.; Gu, C.; Guan, C.; Luo, J.; Fan, H. J. Porous Hydroxide Nanosheets on Preformed Nanowires by Electrodeposition: Branched Nanoarrays for Electrochemical Energy Storage. *Chem. Mater.* **2012**, *24*, 3793−3799.
(33) Kim, C.; Gu, W.; Briceno, M.; Robertson, I. M.; Choi, H.; Kim, K. Copper Nanowires with a Five-Twinned Structure Grown by Chemical Vapor Deposition. *Adv. Mater.* **2008**, *20*, 1859−1863.
(34) Williams, D. B.; Carter, C. B. *Transmission Electron Microscopy: a Textbook for Materials Science*, 1st ed.; Plenum Press: New York, 1996.
(35) Hirsch, P. B.; Howie, A.; Nicholson, R. B.; Pashley, D. W.; Whelan, M. J. *Electron Microscopy of Thin Crystals*; Krieger: New York, 1977.
(36) Luo, P.; Prabhu, S. V.; Baldwin, R. P. Constant Potential Amperometric Detection at a Copper-based Electrode: Electrode Formation and Operation. *Anal. Chem.* **1990**, *62*, 752−755.
(37) Marioli, J. M.; Kuwana, T. Electrochemical Characterization of Carbohydrate Oxidation at Copper Electrodes. *Electrochim. Acta* **1992**, *37*, 1187−1197.
(38) Wei, H.; Sun, J.-J.; Guo, L.; Li, X.; Chen, G.-N. Highly Enhanced Electrocatalytic Oxidation of Glucose and Shikimic Acid at a Disposable Electrically Heated Oxide Covered Copper Electrode. *Chem. Commun.* **2009**, 2842−2844.
(39) Ding, Y.; Wang, Y.; Su, L.; Bellagamba, M.; Zhang, H.; Lei, Y. Electrospun Co3O4 Nanofibers for Sensitive and Selective Glucose Detection. *Biosens. Bioelectron.* **2010**, *26*, 542−548.
(40) Meher, S. K.; Rao, G. R. Archetypal Sandwich-structured CuO for High Performance Non-enzymatic Sensing of Glucose. *Nanoscale* **2013**, *5*, 2089−2099.

DOI: 10.1021/acsami.5b04614
ACS Appl. Mater. Interfaces 2015, 7, 16802−16812